

# Crosstalk between cancer and different cancer stroma subtypes promotes the infiltration of tumor-associated macrophages into the tumor microenvironment of oral squamous cell carcinoma

QIUSHENG SHAN<sup>1</sup>, KIYOFUMI TAKABATAKE<sup>1</sup>, HOTAKA KAWAI<sup>1</sup>, MAY WATHONE OO<sup>1</sup>, SHINTARO SUKEGAWA<sup>1,2</sup>, MASAE FUJII<sup>1</sup>, KEISUKE NAKANO<sup>1</sup> and HITOSHI NAGATSUKA<sup>1</sup>

<sup>1</sup>Department of Oral Pathology and Medicine, Okayama University Graduate School of Medicine, Dentistry and Pharmaceutical Science, Okayama 700-8525; <sup>2</sup>Department of Oral and Maxillofacial Surgery, Kagawa Prefectural Central Hospital, Kagawa 760-8557, Japan

Received March 22, 2022; Accepted April 21, 2022

DOI: 10.3892/ijo.2022.5368

**Abstract.** Tumor-associated macrophages (TAMs) are linked to the progression of numerous types of cancer. However, the effects of the tumor microenvironment (TME) of oral squamous cell carcinoma (OSCC), particularly the cancer stroma on TAMs, remains to be elucidated. In the present study, the effects of verrucous SCC-associated stromal cells (VSCC-SCs), SCC-associated stromal cells (SCC-SCs) and human dermal fibroblasts (HDFs) on the differentiation, proliferation and migration of macrophages *in vitro* was assayed using Giemsa staining, and immunofluorescence, MTS and Transwell (migration) assays, respectively. The combined results suggested that both VSCC-SCs and SCC-SCs promoted the differentiation of macrophages into M2 type TAMs, as well as the proliferation and migration of macrophages following crosstalk with HSC-3 cells *in vitro*. Moreover, the SCC-SCs exerted a more prominent effect on TAMs than the VSCC-SCs. Immunohistochemical staining was used to examine the expression of CD34, CD45, CD11b and CD163 to assay the effects of VSCC-SCs, SCC-SCs and HDFs on microvessel density (MVD) and the infiltration of CD45(+) monocytes, CD11b(+) TAMs and CD163(+) M2 type macrophages. The results suggested that both VSCC-SCs and SCC-SCs promoted MVD and the infiltration of CD45(+) monocytes, CD11b(+) TAMs and CD163(+) M2 type TAMs into the TME of OSCC following crosstalk with HSC-3 cells *in vivo*. The SCC-SCs exerted a more prominent promoting

effect than the VSCC-SCs. Finally, the potential genes underlying the differential effects of VSCC-SCs and SCC-SCs on the infiltration of TAMs were investigated using microarray analysis. The results revealed that interleukin 1 $\beta$ , bone morphogenetic protein 4, interleukin 6 and C-X-C motif chemokine ligand 12 had great potential to mediate the differential effects of VSCC-SCs and SCC-SCs on TAM infiltration. On the whole, the findings presented herein, demonstrate that both VSCC-SCs and SCC-SCs promote the infiltration of TAMs into the TME of OSCC following crosstalk with HSC-3 cells; the SCC-SCs were found to exert a more prominent promoting effect. This may represent a potential regulatory mechanism for the infiltration of TAMs into the TME of OSCC.

## Introduction

Oral squamous cell carcinoma (OSCC) is the most common type of cancer of the head and neck region, occurring in the oral mucosa with a low 5-year survival rate (1,2). The progression of OSCC is dependent on the interplay between cancer cells, the surrounding host-derived stromal cells (SCs), such as cancer-associated fibroblasts (CAFs), endothelial cells, extracellular matrix non-cellular and tumor-associated macrophages (TAMs) composing the tumor microenvironment (TME). Inflammation promotes nearly all stages of OSCC carcinogenesis and progression (3). Recent studies have indicated that macrophages and relevant cytokines are involved in inflammation (4,5). TAM-associated cancer inflammation regulates tumor growth and progression via various mechanisms, depending on the type and frequency of released tumor-derived factors (6,7). Of note, the infiltration of TAMs and their functional activation are key prognostic biomarkers of OSCC lymphangiogenesis, metastatic dissemination and overall survival (8,9).

TAMs are derived from circulating monocytes in the peripheral blood and play a crucial role in cancer progression (10). Macrophages are divided into the M1 (classically activated) and M2 (alternatively activated) phenotypes following polarization (11). M1 macrophages exert antitumor effects by promoting inflammation and immune reactions,

---

*Correspondence to:* Dr Kiyofumi Takabatake, Department of Oral Pathology and Medicine, Okayama University Graduate School of Medicine, Dentistry and Pharmaceutical Science, 2-5-1 Shikata-cho, Kita-ku, Okayama 700-8525, Japan  
E-mail: gmd422094@s.okayama-u.ac.jp

**Key words:** oral squamous cell carcinoma, tumor-associated macrophages, cancer stroma, tumor microenvironment, microvessel density, microarray

whereas M2 macrophages can promote tumor progression through various pathways, such as immunosuppression (12). In OSCC, TAMs primarily exhibit characteristics and functions related to M2 pro-tumor macrophages, and in OSCC, monocyte differentiation into M2 type macrophages can be promoted, which can regulate the progression of OSCC by crosstalk with cancer cells (13,14). Although it has been well established that TAMs play an essential role in tumor immune suppression and progression, the potential regulatory mechanisms of these TAMs with tumor-promoting functions remain unclear (15).

Although it has been reported that OSCC cells recruit TAMs by inducing monocyte differentiation (13), the effects of the cancer stroma on TAM infiltration have not yet been fully elucidated. According to the invasive ability, OSCC is divided into either endophytic (ED) or exophytic (EX) type OSCC. ED-type OSCC can invade and occasionally metastasize. Conversely, EX-type OSCC, such as verrucous OSCC, presents an outward growth, does not invade the subepithelial connective tissue and does not metastasize (16-18). The authors have previously reported that EX-type OSCC-associated SCs [verrucous SCC-associated SCs (VSCC-SCs)] and ED-type OSCC associated SCs (SCC-SCs) exert differential effects on the differentiation, proliferation, invasion and migration of HSC-2 and HSC-3 cells (19,20). In these previous studies, the morphology and viability of VSCC-SCs and SCC-SCs were assayed using Giemsa, immunofluorescence (IF) staining and MTS assays, respectively, which indicated that the VSCC-SCs and SCC-SCs were heterogeneous cell populations and the viability of the VSCC-SCs was higher than that of the SCC-SCs. Different detailed marker profiles between VSCC-SCs and SCC-SCs were also analyzed using microarray data (19,20). However, the effects of VSCC-SCs and SCC-SCs on the infiltration of TAMs into the TME of OSCC remain poorly understood.

The present study thus aimed to investigate the effects of the cancer stroma derived from different subtypes of OSCC on the infiltration of TAMs into the TME of OSCC. To achieve this, the human oral cancer cell line, HSC-3, was selected as the cell model due to it being a moderately or poorly differentiated oral cancer cell line, this cell line also has a prominent invasive ability and can form the stroma more easily and as such, is widely used in studies on TAMs (21,22). In addition, murine RAW264.7 cells were selected as a macrophage cell model; human dermal fibroblasts (HDFs) were selected as a negative control of cancer SCs, mainly since these are a type of normal fibroblasts, which are not affected by cancer cells (23). VSCC-SCs and SCC-SCs were extracted from patients with OSCC to examine their effects on the infiltration/polarization of TAMs into the TME of OSCC and to elucidate the relevant regulatory mechanisms. The findings presented herein highlight a potential regulatory mechanism underlying the effects of cancer-associated stroma on the infiltration of TAMs into the TME of OSCC.

## Materials and methods

**Cells and cell culture.** HSC-3 (JCRB0623), HDFs (CC-2511) and RAW264.7 cells (RCB0535) were purchased from the Japanese Collection of Research Bioresources Cell Bank

(JCRB), Lonza and the RIKEN BioResource Center Cell Bank, respectively. VSCC-SCs and SCC-SCs were extracted from surgical tissues at the Department of Oral and Maxillofacial Surgery at Okayama University (Okayama, Japan). VSCC tissues were obtained from 1 patient with VSCC and SCC tissues were obtained from 1 patient with SCC (mean age, 81 years; sex of both patients, female) to separate the SCs and generate cell culture. Sections of fresh OSCC tissue (1 mm<sup>3</sup>) were washed several times with  $\alpha$ -modified Eagle's medium ( $\alpha$ -MEM; Thermo Fisher Scientific, Inc.) containing antibiotic-antimycotic (Thermo Fisher Scientific, Inc.) and then minced. The tissues were then treated with  $\alpha$ -MEM containing 1 mg/ml collagenase II (Invitrogen; Thermo Fisher Scientific, Inc.) and dispase (Invitrogen; Thermo Fisher Scientific, Inc.) for 2 h at 37°C with agitation (22.36 x g). The released cells were centrifuged for 5 min at 111.8 x g at room temperature, suspended in  $\alpha$ -MEM containing 10% FBS (Biowest), filtered through a cell strainer (100  $\mu$ m; Falcon; Corning Life Sciences), plated in a tissue culture flask and incubated at 37°C in a humidified atmosphere of 5% CO<sub>2</sub> and 95% air. After 1 week, the stromal cells were separated using Accutase (Invitrogen; Thermo Fisher Scientific, Inc.) based on the different adhesive properties of epithelial and stromal cells (19,20). The HSC-3 and RAW264.7 cells, as well as the VSCC-SCs, SCC-SCs and HDFs were maintained in  $\alpha$ -MEM (Thermo Fisher Scientific, Inc.) supplemented with 10% FBS and 1% antimycotic-antibiotic (Thermo Fisher Scientific, Inc.) at 37°C in a humidified atmosphere of 5% CO<sub>2</sub> and 95% air. The present study was approved by the Ethics Committee of Okayama University (project identification code: 1703-042-001). Written informed consent was obtained from all the patients.

**Indirect co-culture.** The VSCC-SCs, SCC-SCs, HDFs, and RAW264.7 and HSC-3 cells were collected using Accutase (Invitrogen; Thermo Fisher Scientific, Inc.) and EDTA (Thermo Fisher Scientific, Inc.), respectively, at 90% confluency. The VSCC-SCs, SCC-SCs and HDFs (15x10<sup>4</sup> cells) were mixed with HSC-3 cells (5x10<sup>4</sup> cells) at a 3:1 ratio in 500  $\mu$ l  $\alpha$ -MEM with 10% FBS and added to a 0.4- $\mu$ m Transwell filter in a 24-well plate (Greiner Bio-One). The RAW264.7 cells were seeded into the bottom chamber in 500  $\mu$ l  $\alpha$ -MEM with 10% FBS at a density of 15x10<sup>4</sup> cells/500  $\mu$ l.

**Giemsa and IF staining.** Following indirect co-culture for 48 h, the RAW264.7 cells in the bottom chamber were collected and seeded into 6-well plates with coverslips (Matsunami Glass, 22x22 mm). Following incubation for 48 h at 37°C in a humidified atmosphere of 5% CO<sub>2</sub> and 95% air, coverslips were used for Giemsa and IF staining. Giemsa staining was conducted using a Giemsa staining kit (Diff-Quick, Nanjing Jiancheng Bioengineering Institute). The slides were first washed with distilled water and fixed with Diff-Quik Fixative provided with the Giemsa staining kit for 2 min at room temperature. Subsequently, the slides were stained with Diff-Quik Solution I and Diff-Quik Solution II provided with the Giemsa staining kit for 2 min at room temperature. The stained cells were photographed using a bright-field microscope (BX51; Olympus Corporation). A total of five images (x20 magnification) were acquired for each sample to determine the percentage of activated macrophages and the percentage of multinucleated giant

cells in the different groups. The independent experiment was repeated in triplicate and the data were analyzed using ImageJ software (V 1.53K; National Institutes of Health).

For IF, the slides were washed three times with TBS (5 min each). The cells were then fixed with 4% paraformaldehyde for 10 min and blocked with blocking solution (DS Pharma Biomedical Co., Ltd.) for 20 min. The primary antibodies rat-anti F4/80 (1:10; cat. no. CI:A3-1, Bio-Rad Laboratories, Inc.) and rabbit-anti CD163 (1: 200; cat. no. ab182422, Abcam) were added followed by incubation for 1 h at room temperature. After washing with TBS three times, the secondary antibodies anti-rat IgG Alexa Fluor 488 (1:200; cat. no. A48262, Thermo Fisher Scientific, Inc.) and anti-rabbit IgG Alexa Fluor 568 (1:200; cat. no. A10042, Thermo Fisher Scientific, Inc.) were added followed by incubation for 1 h at room temperature in the dark. After washing with TBS and distilled water three times, the samples were stained with 0.2 g/ml DAPI (Dojindo Molecular Technologies, Inc.). The stained cells were photographed using an All-in-One BZ-X700 fluorescence microscope (x40 magnification, Keyence Corporation), and independent experiments were repeated in triplicate.

**MTS assay.** Following indirect co-culture for 48 h, RAW264.7 cells in the bottom chamber were collected and seeded into 96-well plates at a density of  $2 \times 10^3$  cells/well. Subsequently, 20  $\mu$ l MTS reagent (Cell Titer 96 Aqueous One Solution Cell Proliferation assay, Promega Corporation) were added to each well followed by incubation for 4 h at 37°C in a humidified atmosphere of 5% CO<sub>2</sub> and 95% air for 1, 2 and 3 days. The absorbance of each well was measured at 490 nm using an ELISA reader (SH-1000 Lab, Corona Electric Co., Ltd.). Independent experiments were repeated in triplicate.

**Transwell (migration) assay and Giemsa staining.** The VSCC-SCs, SCC-SCs, HDFs, and RAW264.7 and HSC-3 cells were collected using Accutase (Invitrogen; Thermo Fisher Scientific, Inc.) and EDTA (Thermo Fisher Scientific, Inc.) at 90% confluency. The VSCC-SCs, SCC-SCs and HDFs ( $1.5 \times 10^4$  cells) were mixed with HSC-3 ( $5 \times 10^4$  cells) cells at a 3:1 ratio in 500  $\mu$ l  $\alpha$ -MEM with 10% FBS and added to the bottom chamber. The RAW264.7 cells were seeded into the upper chamber of 8- $\mu$ m Transwell filters without Matrigel in 24-well plates (Corning, Falcon cell culture inserts; BD Biosciences) in  $\alpha$ -MEM without FBS at a density of  $2 \times 10^4$  cells/500  $\mu$ l. Following incubation for 1 day at 37°C in a humidified atmosphere of 5% CO<sub>2</sub> and 95% air, the upper chambers were stained using the Giemsa staining kit (Diff-Quick, Nanjing Jiancheng Bioengineering Institute). The chambers were first washed with distilled water and fixed with Diff-Quik Fixative provided with the Giemsa staining kit for 2 min at room temperature. Subsequently, the slides were stained with Diff-Quik Solution I and Diff-Quik Solution II provided with the Giemsa staining kit for 2 min at room temperature. The stained cells were photographed using a bright-field microscope (BX51; Olympus Corporation). A total of five images (x20 magnification) were acquired for each sample to assay the cell migration number. Independent experiments were repeated in triplicate and the data were analyzed using ImageJ software (V 1.53K; National Institutes of Health).

**Experimental animals.** All animal experiments were conducted in accordance with the relevant guidelines and regulations approved by the Institutional Committee at Okayama University (OKU-2017406). The anesthesia protocol was performed according to the Laboratory Animal Anesthesia 3rd edition (24,25). Following intraperitoneal anesthesia with ketamine hydrochloride (75 mg/kg body weight) and medetomidine hydrochloride (0.5 mg/kg body weight), the mice were determined to be appropriately anesthetized by whether they would return to a prone position when they were placed on their backs. Subsequently, 200  $\mu$ l mixed cells, including HSC-3 cells ( $1 \times 10^6$  cells, 100  $\mu$ l) and SCs (VSCC-SCs, SCC-SCs and HDFs,  $3 \times 10^6$  cells, 100  $\mu$ l) were injected into the subcutaneous tissue in the central region of the top of the head of 20 healthy female BALB-c nu-nu mice (age, 4 weeks; mean weight, 15 g; Shimizu Laboratory Supplies Co., Ltd.) gradually and slowly, as previously described (26). All mice were reared in an animal room at 25°C with 50-60% humidity under a 12-h light/dark cycle and were provided with free access to food and water. The animal health and behavior were examined by the staff at the animal center once/per day. Any difficulties in eating and water intake, any symptoms of agony (self-harm, abnormal posture, respiratory distress, crying), the long-term appearance of abnormalities with no signs of recovery (diarrhea, bleeding, dirt on the genital area), if the animal's distress was judged to be intolerable, such as heavy weight loss ( $\geq 20\%$  within a few days) or in the case that the transplanted cancer cells grew to a size of  $\geq 3$  cm, were used as the humanitarian endpoints of the study and the experiment was immediately terminated and the animal was euthanized. After 4 weeks, all mice were sacrificed by isoflurane excess inhalation anesthesia (concentration  $> 5\%$ ). Cardiac arrest was then verified by pulse palpation followed by the dislocation of the cervical spine of the mice. The experimental animals were divided into the HSC-3, HSC-3 + VSCC-SCs, HSC-3 + SCC-SCs and HSC-3 + HDFs groups and each group contained 5 mice with tumor formation (n=5 per group). Of the 5 mice per group, 1 mouse in each group exhibited poor tumor formation; therefore, their data were removed and the data from the remaining 4 mice were used for analysis.

**Immunohistochemistry (IHC).** Following antigen retrieval in a microwave for 1 or 8 min in 0.01 M tri-sodium citrate buffer (pH 6) and 0.01 M Dako Target Retrieval Solution (pH 9; cat. no. S2367; Agilent Technologies, Inc.), 5- $\mu$ m-thick sections were blocked with 10% normal serum for 20 min at room temperature and incubated with primary antibodies, including rabbit anti-CD34 (1:500; cat. no. ab81289, Abcam), anti-CD45 (1:200; cat. no. ab10558, Abcam), anti-CD11b (1:1,000; cat. no. ab133357, Abcam) and anti-CD163 (1:200; cat. no. ab182422, Abcam) overnight at 4°C. After washing three times with TBS, all sections were incubated with avidin-biotin complexes (PK-6101, rabbit ABC kit; Vector Laboratories, Inc.) for 1 h at room temperature. Following visualization using DAB/H<sub>2</sub>O<sub>2</sub> mixed solution (Histofine DAB substrate; Nichirei Corporation), the skin invasion front and bottom invasion front of the tissues were photographed using a bright field microscope (BX51; Olympus Corporation). A total of ten images (x40 magnification) were acquired for each mouse to assay the expression of CD34, CD45, CD11b and CD163

using IHC scoring with ImageJ software (V 1.53K; National Institutes of Health). The IHC score = the score of percentage of positive cells  $\times$  the score of intensity. The score of percentage of positive cells was classified as follows: 0 (<1%), 1 (1-24%), 2 (25-49%), 3 (50%-74%) and 4 (75-100%). The score of intensity were classified as follows: 0, no staining; 1, light yellow (weak staining); 2, brown (moderate strong staining); and 3, dark brown (strong staining) (27). The microvessel density (MVD) in the central area was assayed by calculating the CD34(+) vessel structure in each image (positive area/image).

**Microarray and bioinformatics analyses.** Microarray and bioinformatics methods were used to identify the potential genes involved in the differential effects of VSCC-SCs and SCC-SCs on the infiltration of TAMs into the TME of OSCC. GeneSpring GX 14.9 (Agilent Technologies, Inc.) software was used to determine the differentially expressed genes (DEGs) in SCC-SCs compared with those in VSCC-SCs. A  $|\text{LogFC}| > 1$  was considered the cut-off value (the dataset was uploaded onto the Gene Expression Omnibus database, <https://www.ncbi.nlm.nih.gov/geo/query/acc.cgi?acc=GSE164374>). The biological process of upregulated DEGs was examined by Gene Ontology (GO) enrichment analysis using Cytoscape 3.7.2 (<https://cytoscape.org/>); an adjusted  $P < 0.05$  was considered as the cut-off value. The hub genes in vessel formation-associated biological processes and TAM-associated biological processes were identified using a protein-to-protein interaction network (PPI) with STRING (<http://string-db.org/>) and Cytoscape 3.7.2 (cytohubba) software. A combined score  $> 0.4$  was considered as the cut-off value and the hub genes were selected according to the degree. The common hub genes between vessel formation-associated biological processes and TAM-associated biological processes were identified using Venn (a software plug-in within SangerBox; <http://sangerbox.com>). These common hub genes could not be detected in the animal models as the VSCC-SCs and SCC-SCs disappeared gradually after the injection. Given that the microarray data already represented the actual mRNA expression level in VSCC-SCs and SCC-SCs, the protein expression level of these common hub genes was not further confirmed.

**Statistical analysis.** Statistical analysis was conducted using GraphPad Prism 9 (GraphPad Software, Inc.). The cell experiments were repeated in triplicate and the animal experiments were repeated using 5 independent mice. The parametric data are presented as the mean  $\pm$  SD and were analyzed by ordinary one-way ANOVA followed by Tukey's post hoc test. The non-parametric data are presented as the median and interquartile range (IQR) and were analyzed using the Kruskal-Wallis test followed by Dunn's test. A value of  $P < 0.05$  was considered to indicate a statistically significant difference.

## Results

*Crosstalk between SCC-SCs and HSC-3 cells exerts a more prominent promoting effect on the activation and fusion of macrophages than VSCC-SCs in vitro.* Following indirect co-culture, Giemsa staining was used to examine the morphology of the macrophages in the different groups to determine the effects of VSCC-SCs and SCC-SCs on

the activation and fusion of macrophages (Fig. 1A). The percentage of activated macrophages in the RAW264.7 + SCC-SCs group was the highest, followed by the RAW264.7 + VSCC-SCs group. Only minimal differences were observed between the RAW264.7 and RAW264.7 + HDFs groups (Fig. 1C). Following crosstalk with HSC-3 cells *in vitro*, the percentage of activated macrophages in the RAW264.7 + HSC-3 + SCC-SCs group was slightly higher than that in the RAW264.7 + HSC-3 + VSCC-SCs and markedly higher than the RAW264.7 + HSC-3 and RAW264.7 + HSC-3 + HDFs groups. Only minimal differences were observed between the RAW264.7 + HSC-3 and RAW264.7 + HSC-3 + HDFs groups (Fig. 1D). The percentage of multinucleated giant cells in the RAW264.7 + SCC-SCs group was the highest, followed by the RAW264.7 + VSCC-SCs group. Only a minimal difference was observed between the RAW264.7 group and RAW264.7 + HDFs group. (Fig. 1E). Following crosstalk with HSC-3 cells *in vitro*, the percentage of multinucleated giant cells in the RAW264.7 + HSC-3 + SCC-SCs was higher than that in the RAW264.7 + HSC-3 + VSCC-SCs and RAW264.7 + HSC-3 + HDFs groups, and was markedly higher than that in the RAW264.7 + HSC-3 group (Fig. 1F). Furthermore, IF staining was used to examine the expression of F4/80 and CD163 in the different groups to determine the characteristics of activated macrophages and multinucleated giant cells. These two cell types were mainly F4/80(+) and CD163(+), indicating that the characteristics of these cells were similar to those of M2 type macrophages (Fig. 1B). These data suggest that both VSCC-SCs and SCC-SCs promoted the activation and fusion of macrophages following crosstalk with HSC-3 cells *in vitro* and that the SCC-SCs exerted a more prominent promoting effect than the VSCC-SCs, while the HDFs had a minimal effect.

*Crosstalk between SCC-SCs and HSC-3 cells exerts a more prominent promoting effect on the proliferation of macrophages than VSCC-SCs in vitro.* Following indirect co-culture, MTS assay was used to examine the proliferative ability of different groups to assay the effects of VSCC-SCs, SCC-SCs and HDFs on the proliferation of macrophages *in vitro*. On day 1, the optical density (OD) value in the RAW264.7 + HDFs group was slightly higher than that in the RAW264.7 + SCC-SCs and RAW264.7 + VSCC-SCs groups, and markedly higher than that in the RAW264.7 group. There was a minimal difference between the RAW264.7 + VSCC-SCs and RAW264.7 + SCC-SCs groups (Fig. 2A). Following crosstalk with the HSC-3 cells *in vitro*, the OD value in the RAW264.7 + HSC-3 + HDFs group was the highest, followed by that in the RAW264.7 + HSC-3 + SCC-SCs group. The OD value of the RAW264.7 + HSC-3 group was slightly higher than that of the RAW264.7 + VSCC-SCs group (Fig. 2B). On day 2, the OD value in the RAW264.7 + HDFs and RAW264.7 groups was slightly higher than that in the RAW264.7 + VSCC-SCs group, and markedly higher than that in the RAW264.7 + SCC-SCs group. Only a minimal difference was observed between the RAW264.7 and RAW264.7 + HDFs groups (Fig. 2C). Following crosstalk with HSC-3 cells *in vitro*, the OD value in the RAW264.7 + HSC-3 + SCC-SCs group was the highest, followed by the RAW264.7 + HSC-3 + HDFs group. The OD value in the RAW264.7 + HSC-3 + VSCC-SCs

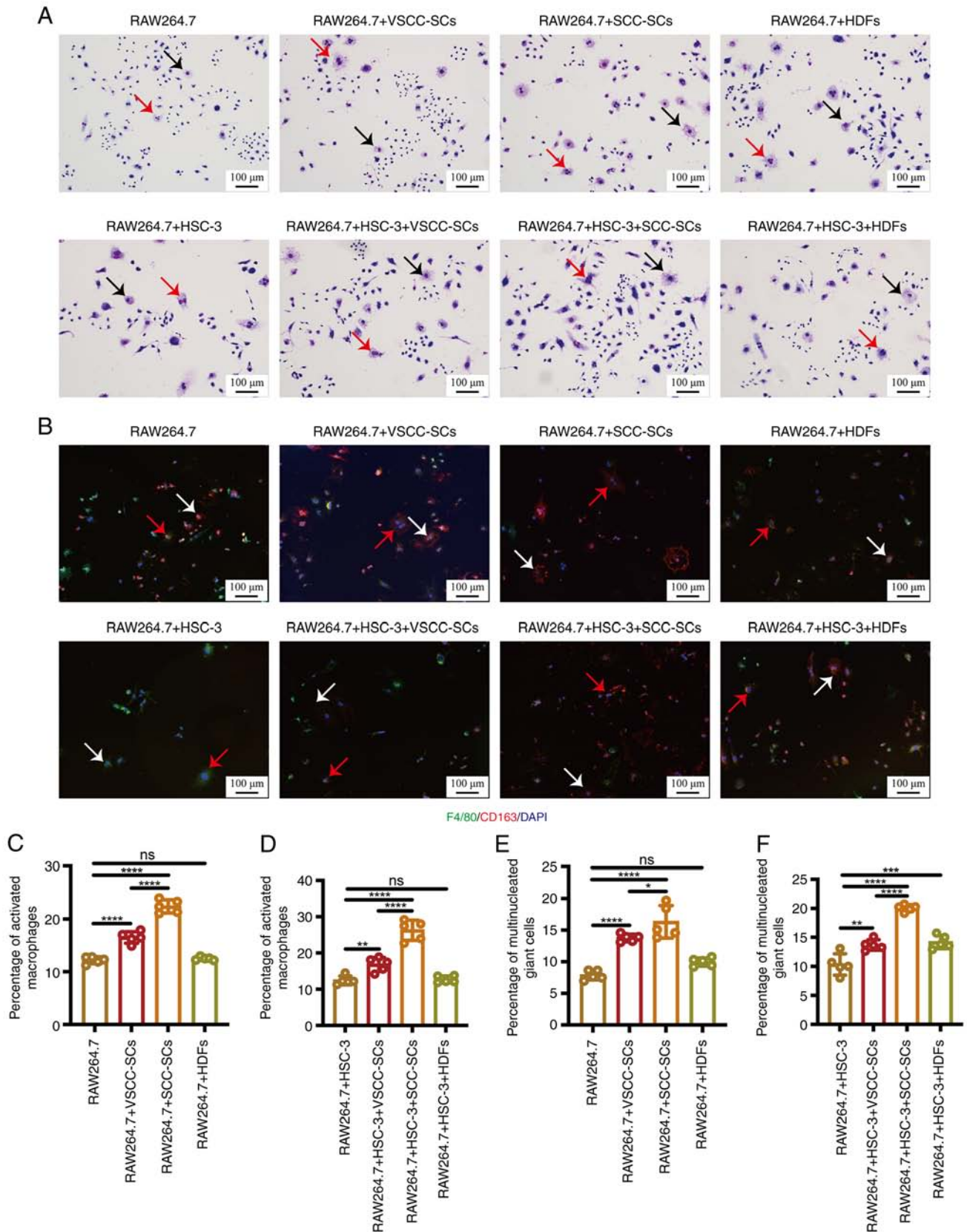


Figure 1. Effects of VSCC-SCs, SCC-SCs and HDFs on the activation and fusion of macrophages following crosstalk with HSC-3 cells *in vitro*. (A) Giemsa staining was used to examine the effects of VSCC-SCs, SCC-SCs and HDFs on the activation and fusion of macrophages following crosstalk with HSC-3 cells *in vitro*. Black arrows indicate activated macrophages and red arrows indicate multinucleated giant cells. (B) Immunofluorescence staining was used to examine F4/80 and CD163 expression to identify the characteristics of activated macrophages and multinucleated giant cells. White arrows indicate activated macrophages and red arrow indicate multinucleated giant cells. Quantification of (C and D) the percentage of activated macrophages and (E and F) the percentage of multinucleated giant cells in the different groups. Data are presented as the mean  $\pm$  SD of one independent experiment and the independent experiments were repeated in triplicate. Statistical analysis was performed using one-way ANOVA followed by Tukey's post hoc test. \* $P < 0.05$ , \*\* $P < 0.01$ , \*\*\* $P < 0.001$  and \*\*\*\* $P < 0.0001$ . ns, not significant ( $P > 0.05$ ); VSCC-SCs, verrucous squamous cell carcinoma-associated stromal cells; SCC-SCs, squamous cell carcinoma-associated stromal cells; HDFs, human dermal fibroblasts.

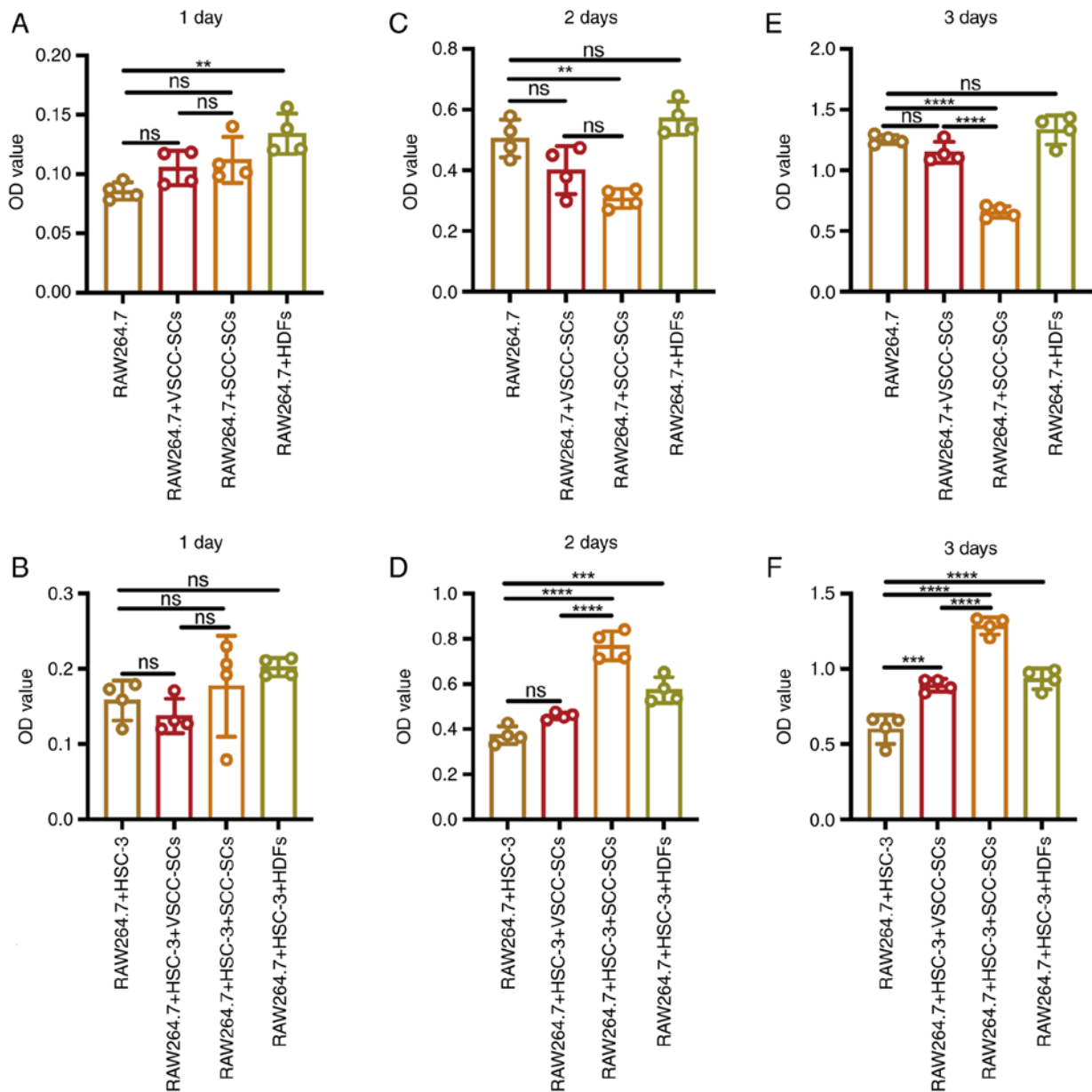


Figure 2. Effects of VSCC-SCs, SCC-SCs and HDFs on the proliferation of macrophages following crosstalk with HSC-3 cells *in vitro*. (A, C and E) MTS assay was used to examine the proliferative ability in the different groups to assay the effects of VSCC-SCs, SCC-SCs and HDFs on the proliferation of macrophages *in vitro* on day (A) 1, (C) day 2 and (E) day 3. (B, D and F) MTS assay was used to examine the proliferative ability in the different groups to assay the effects of VSCC-SCs, SCC-SCs and HDFs on the proliferation of macrophages following crosstalk with HSC-3 cells *in vitro* on (B) day 1, (D) day 2 and (F) day 3. Data are presented as the mean  $\pm$  SD of one independent experiment and the independent experiments were repeated in triplicate. Statistical analysis was performed using one-way ANOVA followed by Tukey's post hoc test. \*\* $P < 0.01$ , \*\*\* $P < 0.001$  and \*\*\*\* $P < 0.0001$ . ns, not significant ( $P > 0.05$ ); VSCC-SCs, verrucous squamous cell carcinoma-associated stromal cells; SCC-SCs, squamous cell carcinoma-associated stromal cells; HDFs, human dermal fibroblasts.

group was slightly higher than that in the RAW264.7 + HSC-3 group (Fig. 2D). On day 3, the OD value in the RAW264.7 and RAW264.7 + HDFs groups was slightly higher than that in the RAW264.7 + VSCC-SCs group and markedly higher than that in the RAW264.7 + SCC-SCs group. There was only a minimal difference between the RAW264.7 and RAW264.7 + HDFs groups (Fig. 2E). Following crosstalk with HSC-3 cells, the OD value in the RAW264.7 + HSC-3 + SCC-SCs group was the highest, followed by the RAW264.7 + HSC-3 + HDFs group. The OD value of the RAW264.7 + HSC-3 + VSCC-SCs group was slightly higher than that of the RAW264.7 + HSC-3 group (Fig. 2F). These data suggested that both the VSCC-SCs and SCC-SCs inhibited the proliferation of macrophages *in vitro*,

and that the SCC-SCs exerted a more prominent inhibitory effect than the VSCC-SCs. Following crosstalk with HSC-3 cells, both the VSCC-SCs and SCC-SCs promoted the proliferation of macrophages *in vitro*, and the SCC-SCs exerted a more prominent promoting effect than the VSCC-SCs.

*Both VSCC-SCs and SCC-SCs promote the migration of macrophages via crosstalk with HSC-3 cells in vitro.* Transwell (migration) and Giemsa staining were used to examine the effects of VSCC-SCs and SCC-SCs on the migration of macrophages *in vitro*. The cell migration number in the RAW264.7 + SCC-SCs group was slightly lower than that in the other groups, and there was only a minimal difference between

the other three groups. All the four groups mainly contained spindle-shaped macrophages and several round-shaped macrophages could also be observed (Fig. 3A and C). The cell migration number in the RAW264.7 + HSC-3 + SCC-SCs and RAW264.7 + HSC-3 + VSCC-SCs groups was slightly higher than that in the RAW264.7 + HSC-3 group and markedly higher than that in the RAW264.7 + HSC-3 + HDFs group, and there was a minimal difference between the RAW264.7 + HSC-3 + SCC-SCs and RAW264.7 + HSC-3 + VSCC-SCs groups (Fig. 3B and D). The RAW264.7 + HSC-3 and RAW264.7 + HSC-3 + HDFs groups mainly contained spindle-shaped macrophages and several round-shaped macrophages could also be observed, while the RAW264.7 + HSC-3 + VSCC-SCs group primarily contained round-shaped macrophages and spindle-shaped macrophages. The RAW264.7 + HSC-3 + SCC-SCs group mainly contained round-shaped macrophages (Fig. 3B). Therefore, both the VSCC-SCs and SCC-SCs promoted the migration and changes in the shape of macrophages following crosstalk with HSC-3 cells *in vitro*, and the SCC-SCs exerted a more prominent effect on changes in the shape of macrophages than the VSCC-SCs following crosstalk with HSC-3 cells *in vitro*.

*Crosstalk between SCC-SCs and HSC-3 cells exerts a more prominent promoting effect on the MVD in the TME of OSCC than VSCC-SCs in vivo.* Given that the macrophages were derived from blood, IHC staining was used to examine CD34 expression to determine the effects of VSCC-SCs, SCC-SCs and HDFs on the MVD in the TME of OSCC. In the skin invasion front, the IHC score in the HSC-3 + SCC-SCs group was higher than that in the HSC-3 + VSCC-SCs group, and markedly higher than that in the HSC-3 and HSC-3 + HDFs groups. The IHC score in the HSC-3 + HDFs group was higher than that in the only HSC-3 group (Fig. 4A and B). In the central area, the positive area/image in the HSC-3 + SCC-SCs group was higher than that in HSC-3 + VSCC-SCs group, and markedly higher than that in the HSC-3 and HSC-3 + HDFs groups. There was a minimal difference between the HSC-3 and HSC-3 + HDFs groups. In addition, the size of the vessels in the HSC-3 + SCC-SCs group was slightly larger than that in the HSC-3 + VSCC-SCs group and markedly larger than that in the HSC-3 and HSC-3 + HDFs groups based on the length of MVD (Fig. 4C and D). At the bottom invasion front, the IHC score in the HSC-3 + SCC-SCs group was higher than that in the HSC-3 + VSCC-SCs group and markedly higher than that in HSC-3 and HSC-3 + HDFs groups. The IHC score in the HSC-3 + HDFs group was slightly higher than that in the only HSC-3 group (Fig. 4E and F). Thus, these data demonstrated that both the VSCC-SCs and SCC-SCs promoted the MVD in the TME of OSCC following crosstalk with HSC-3, and the SCC-SCs exerted a more prominent promoting effect than the VSCC-SCs, while the HDFs had a minimal promote effect in the skin and bottom invasion fronts.

*Crosstalk between SCC-SCs and HSC-3 cells exerts a more prominent promoting effect on the infiltration of CD45(+) monocytes into the TME of OSCC than VSCC-SCs in vivo.* Given that the macrophages were derived from monocytes from peripheral blood, IHC staining was used to examine CD45 expression to determine the effects of VSCC-SCs,

SCC-SCs and HDFs on the infiltration of CD45(+) monocytes into the TME of OSCC. In the skin invasion front, the IHC score of CD45 in HSC-3 + SCC-SCs group was higher than that in HSC-3 + VSCC-SCs group, and markedly higher than that in the HSC-3 and HSC-3 + HDFs groups. There was a minimal difference between the HSC-3 and HSC-3 + HDFs groups (Fig. 5A and C). In the bottom invasion front, the IHC score of CD45 in the HSC-3 + VSCC-SCs and HSC-3 + SCC-SCs group was slightly higher than that in the HSC-3 + HDFs group, and markedly higher than that in the HSC-3 group. There was a minimal difference between the HSC-3 + VSCC-SCs and HSC-3 + SCC-SCs groups (Fig. 5B and D). Therefore, both the VSCC-SCs and SCC-SCs promoted the infiltration of CD45(+) monocytes into the TME of OSCC, and the SCC-SCs exerted a more prominent promoting effect than the VSCC-SCs, while the HDFs exerted a minimal effect.

*Crosstalk between SCC-SCs and HSC-3 cells exerts a more prominent promoting effect on the infiltration of CD11b(+) pre-macrophages and macrophages (M0 type macrophages) into the TME of OSCC than VSCC-SCs in vivo.* Given that pre-macrophages [bone marrow-derived cells (BMDCs)] and macrophages are CD11b(+), IHC staining was used to observe CD11b expression to determine the effects of VSCC-SCs, SCC-SCs and HDFs on the infiltration of CD11b(+) M0 type macrophages into the TME of OSCC. In the skin invasion front, the IHC score of CD11b in the HSC-3 + SCC-SCs group was the highest, followed by that in the HSC-3 + VSCC-SCs group. There was a minimal difference between the HSC-3 and HSC-3 + HDFs groups (Fig. 6A and C). At the bottom invasion front, the IHC score of CD11b in the HSC-3 + SCC-SCs group was higher than that in the HSC-3 + VSCC-SCs group, and markedly higher than that in the HSC-3 and HSC-3 + HDFs groups. There was a minimal difference between the HSC-3 and HSC-3 + HDFs groups (Fig. 6B and D). Therefore, both the VSCC-SCs and SCC-SCs promoted the infiltration of CD11b(+) M0 type macrophages into the TME of OSCC, and SCC-SCs exerted a more prominent promoting effect than the VSCC-SCs, while the HDFs exerted a minimal effect.

*Crosstalk between SCC-SCs and HSC-3 cells exerts a more prominent promoting effect on the infiltration of CD163(+) M2 type TAMs into the TME of OSCC than VSCC-SCs in vivo.* IHC staining was used to examine CD163 expression to assay the effects of VSCC-SCs, SCC-SCs and HDFs on the infiltration of CD163(+) M2 type TAMs into the TME of OSCC. In the skin invasion front, the IHC score of CD163 in the HSC-3 + SCC-SCs group was the highest, followed by that in the HSC-3 + VSCC-SCs group. There was a minimal difference between the HSC-3 and HSC-3 + HDFs groups (Fig. 7A and C). At the bottom invasion front, there were negative results in these four groups (Fig. 7B). Therefore, both the VSCC-SCs and SCC-SCs promoted the infiltration of CD163(+) M2 type TAMs into the TME of OSCC via crosstalk with HSC-3, and the SCC-SCs exerted a more prominent promoting effect than the VSCC-SCs, while the HDFs exerted a minimal effect.

*IL1B, BMP4, IL6 and CXCL12 may be involved in the differential effects of VSCC-SCs and SCC-SCs on the infiltration of TAMs into the TME of OSCC.* The DEGs in

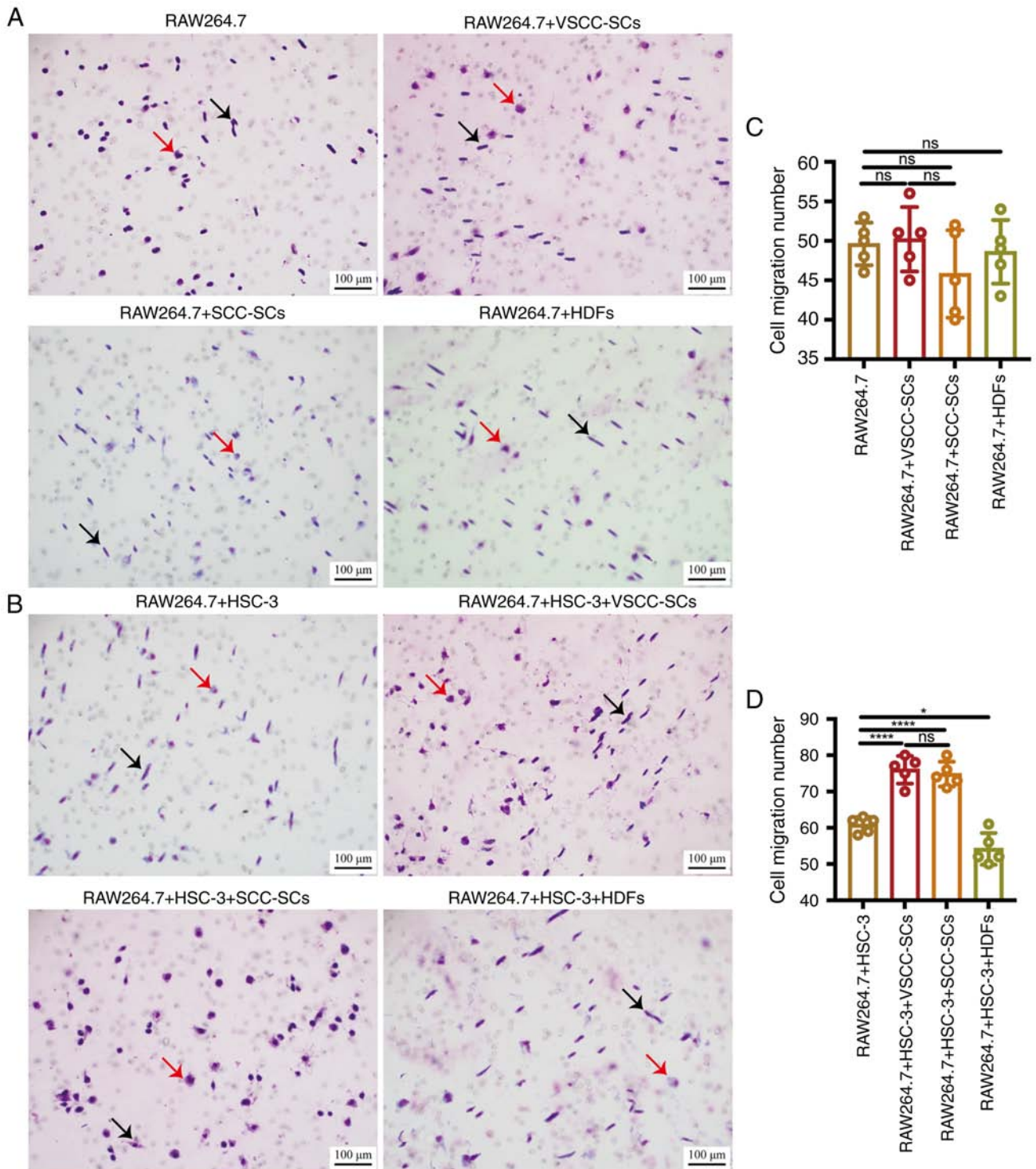


Figure 3. Effects of VSCC-SCs, SCC-SCs and HDFs on the migration of macrophages following crosstalk with HSC-3 cells *in vitro*. (A) Transwell (migration) and Giemsa staining were used to examine the effects of VSCC-SCs, SCC-SCs and HDFs on the migration of macrophages. Black arrows indicate spindle-shaped macrophages and red arrows indicate round-shaped macrophages. (B) Transwell (migration) and Giemsa staining were used to examine the effects of VSCC-SCs, SCC-SCs and HDFs on the migration of macrophages following crosstalk with HSC-3 cells *in vitro*. Black arrows indicate spindle-shaped macrophages and red arrows indicate round-shaped macrophages. (C and D) Quantification of cell migration number in the different groups. Data are shown as the mean  $\pm$  SD of one independent experiment and the independent experiments were repeated in triplicate. Statistical analysis was performed using one-way ANOVA followed by Tukey's post hoc test. \* $P < 0.05$  and \*\*\*\* $P < 0.0001$ . ns, not significant ( $P > 0.05$ ); VSCC-SCs, verrucous squamous cell carcinoma-associated stromal cells; SCC-SCs, squamous cell carcinoma-associated stromal cells; HDFs, human dermal fibroblasts.

the SCC-SCs were compared with those in VSCC-SCs using microarray analysis. The biological process of upregulated DEGs in SCC-SCs was analyzed using GO enrichment analysis, which indicated that these up-DEGs are primarily

enriched in vessel formation-associated biological processes, such as vasculature development and blood vessel development (Fig. 8A), as well as TAM-associated biological processes, such as cell migration and cell motility (Fig. 8B).

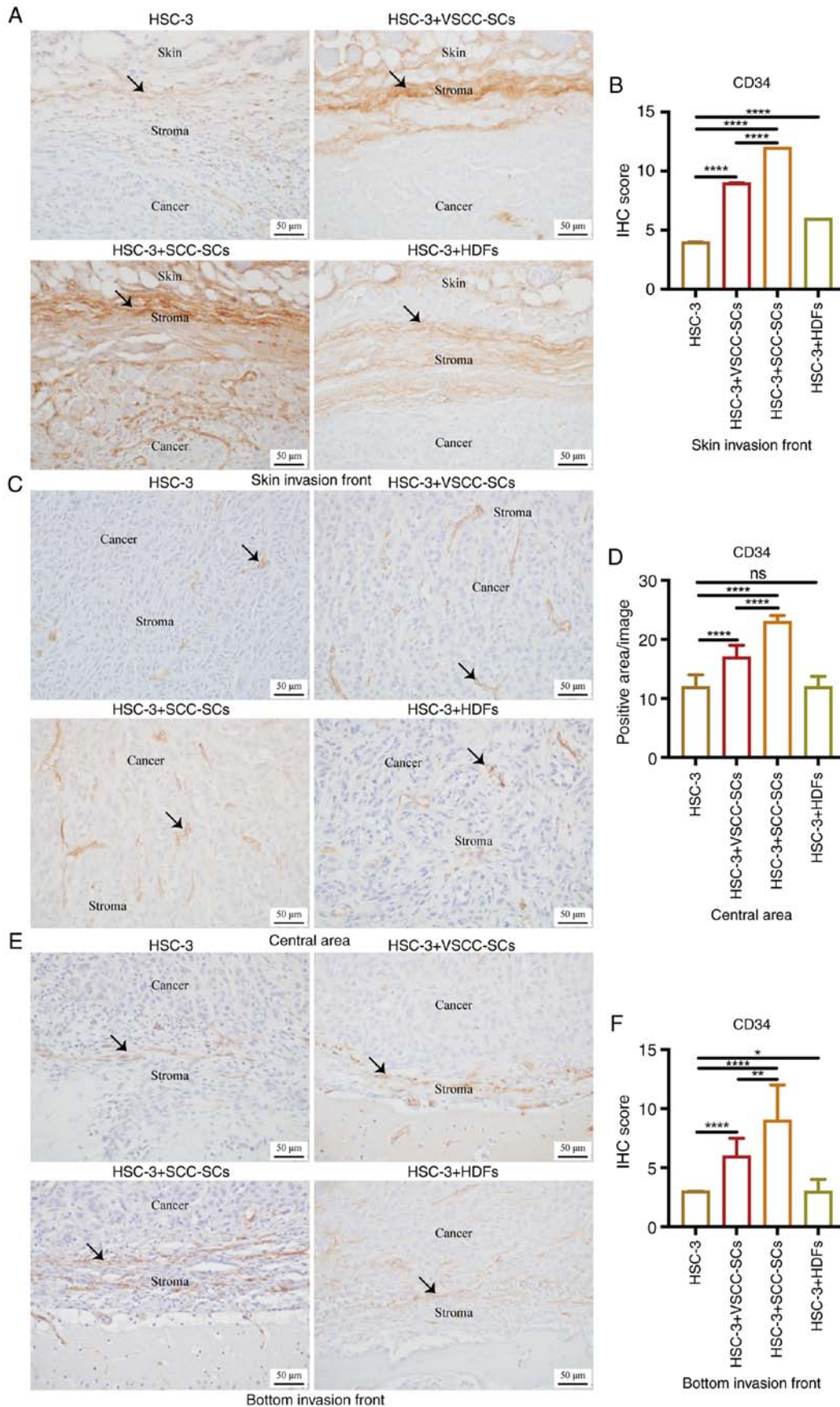


Figure 4. Effects of VSCC-SCs, SCC-SCs and HDFs on the MVD in the tumor microenvironment of OSCC following crosstalk with HSC-3 cells *in vivo*. (A, C and E) Immunohistochemical staining was used to examine the expression of CD34 in the (A) skin invasion front, (C) central area and (E) bottom invasion front. Black arrows indicate vessel structure. (B, D and F) Quantification of CD34 expression in the (B) skin invasion front, (D) central area and (F) bottom invasion front in the different groups. Data are presented as the median and IQR, n=4. Statistical analysis was performed using the Kruskal-Wallis test followed by Dunn's test. \*P<0.05, \*\*P<0.01 and \*\*\*\*P<0.0001. ns, not significant (P>0.05); VSCC-SCs, verrucous squamous cell carcinoma-associated stromal cells; SCC-SCs, squamous cell carcinoma-associated stromal cells; HDFs, human dermal fibroblasts.

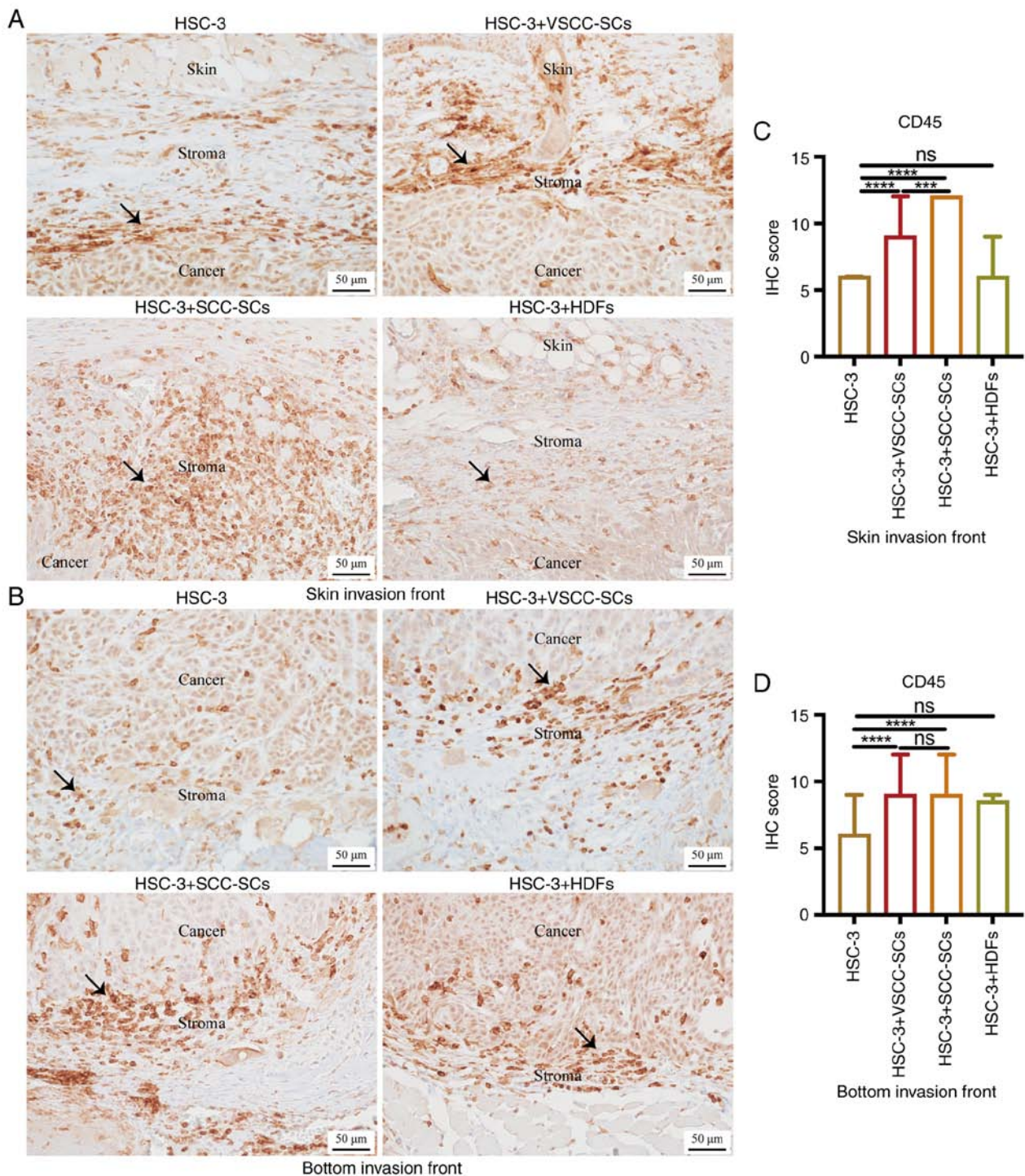


Figure 5. Effects of VSCC-SCs, SCC-SCs and HDFs on the infiltration of CD45(+) monocytes into the tumor microenvironment of OSCC following crosstalk with HSC-3 cells *in vivo*. (A and B) Immunohistochemical staining was used to examine the CD45 expression level to assay the effects of VSCC-SCs, SCC-SCs and HDFs on the infiltration of CD45(+) monocytes in the (A) skin and (B) bottom invasion fronts of oral squamous cell carcinoma, respectively following crosstalk with HSC-3 cells *in vivo*. Black arrows indicate CD45(+) monocytes. (C and D) Quantification of the CD45 expression level in the (C) skin and (D) bottom invasion fronts in the different groups. Data are presented as the median and IQR, n=4. Statistical analysis was performed using the Kruskal-Wallis test followed by Dunn's test. \*\*\*P<0.001 and \*\*\*\*P<0.0001. ns, not significant (P>0.05); VSCC-SCs, verrucous squamous cell carcinoma-associated stromal cells; SCC-SCs, squamous cell carcinoma-associated stromal cells; HDFs, human dermal fibroblasts.

Furthermore, the hub genes in the vessel formation-associated biological processes and TAM-associated biological processes were analyzed by PPI, which suggested that interleukin (IL)6, C-X-C motif chemokine ligand 12 (CXCL12), bone morphogenetic protein 4 (BMP4), forkhead box O1 (FOXO1), nuclear factor of activated T-cells 1 (NFATC1), early growth response

protein 1 (EGR1), low density lipoprotein receptor (LDLR), IL1B, Wnt family member 2 (WNT2) and Fms related receptor tyrosine kinase 1 (FLT1) were hub genes in vessel formation-associated biological processes (Fig. 8C), and IL1B, BMP4, intercellular adhesion molecule 1 (ICAM1), IL6, cell division cycle 42 (CDC42), insulin (INS), nerve growth factor

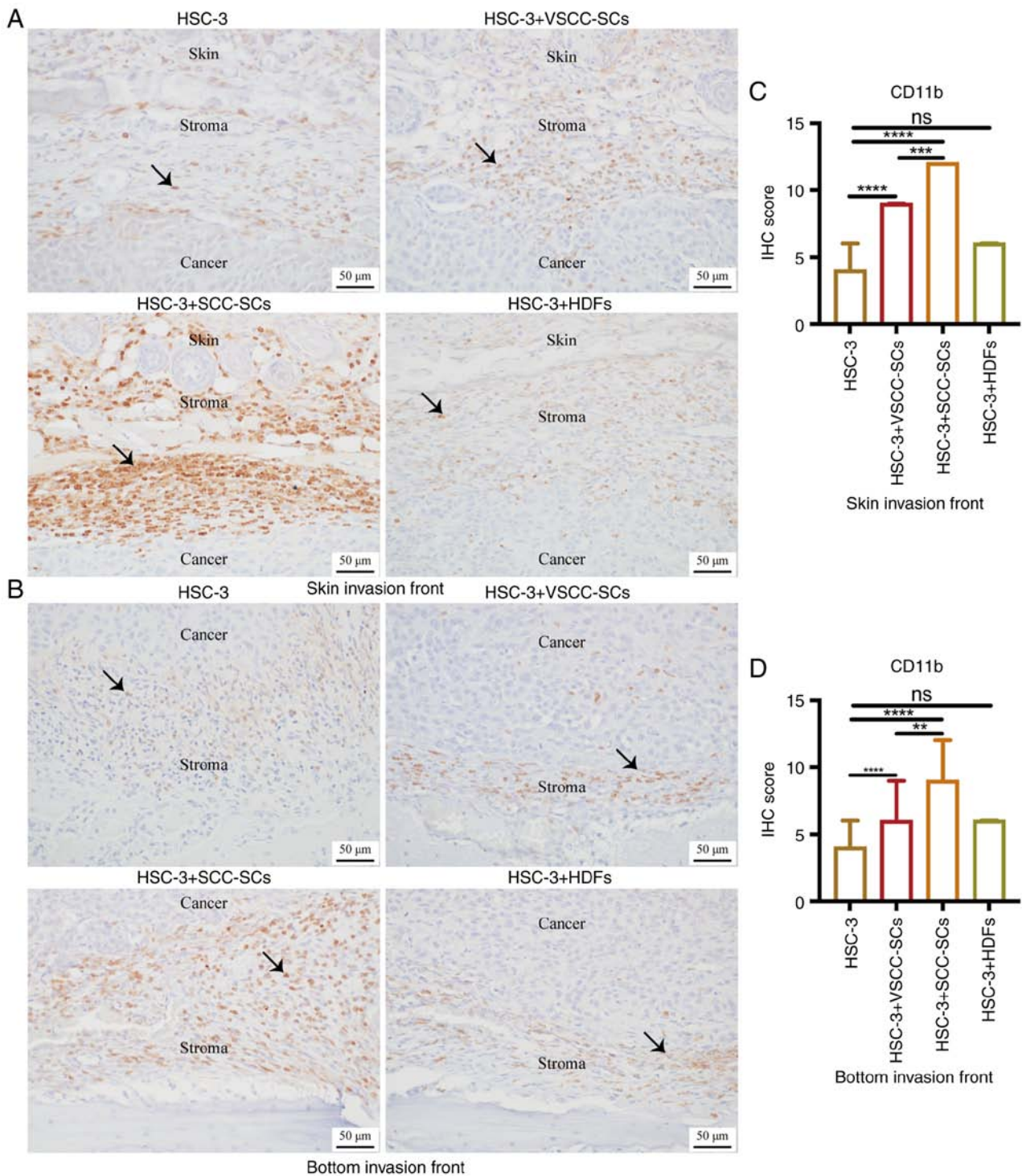


Figure 6. Effects of VSCC-SCs, SCC-SCs and HDFs on the infiltration of CD11b(+) M0 type macrophages into the tumor microenvironment of OSCC following crosstalk with HSC-3 cells *in vivo*. (A and B) Immunohistochemical staining was used to examine the CD11b expression level to assay the effects of VSCC-SCs, SCC-SCs and HDFs on the infiltration of CD11b(+) M0 type macrophages in the (A) skin and (B) bottom invasion fronts of OSCC, respectively following crosstalk with HSC-3 cells *in vivo*. Black arrows indicated the CD11b(+) M0 type macrophages. (C and D) Quantification of CD11b expression level in the (C) skin and (D) bottom invasion fronts in the different groups, respectively. Data are presented as the median and IQR, n=4. Statistical analysis was performed using the Kruskal-Wallis test followed by Dunn's test. \*\*P<0.01, \*\*\*P<0.001 and \*\*\*\*P<0.0001. ns, not significant (P>0.05); OSCC, oral squamous cell carcinoma; VSCC-SCs, verrucous squamous cell carcinoma-associated stromal cells; SCC-SCs, squamous cell carcinoma-associated stromal cells; HDFs, human dermal fibroblasts.

(NGF), Toll-like receptor 4 (TLR4), CXCL12 and cadherin 1 (CDH1) were hub genes in TAM-associated biological processes (Fig. 8D). The common hub genes between them were identified using Venn diagrams, which suggested that IL6, CXCL12, IL1B and BMP4 were common hub genes in

both vessel formation-associated biological processes and TAM-associated biological processes (Fig. 8E). Thus, IL1B, BMP4, IL6 and CXCL12 may be involved in the differential effects of VSCC-SCs and SCC-SCs on the infiltration of TAMs into the TME of OSCC.

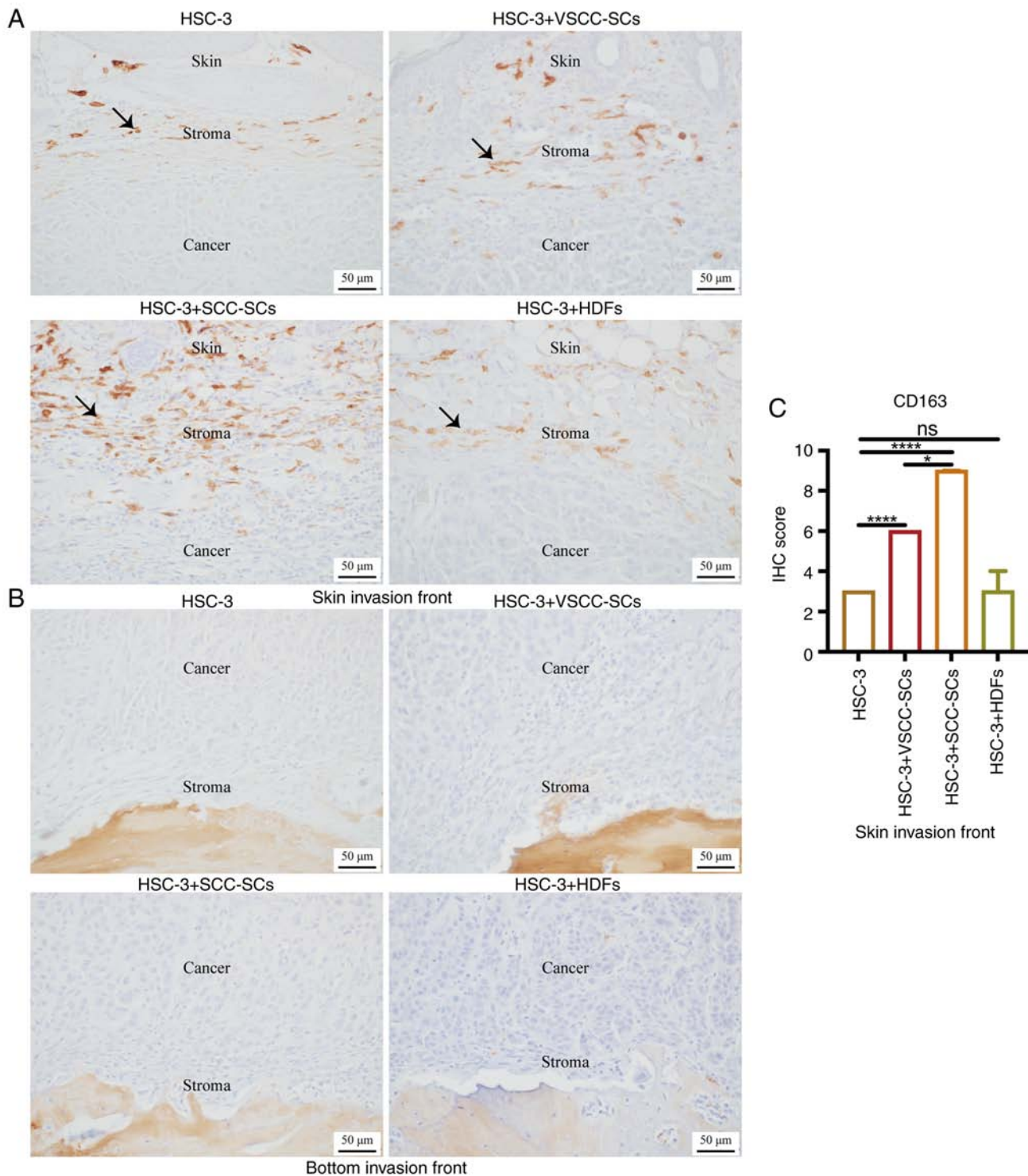


Figure 7. Effects of VSCC-SCs, SCC-SCs and HDFs on the CD163(+) M2 type TAMs into the tumor microenvironment of OSCC following crosstalk with HSC-3 cells *in vivo*. A and B IHC staining was used to test the CD163 expression level to assay the effects of VSCC-SCs, SCC-SCs and HDFs on the infiltration of CD163(+) M2 type TAMs into the (A) skin and (B) bottom invasion fronts of OSCC, respectively following crosstalk with HSC-3 cells *in vivo*. Black arrows indicate CD163(+) M2 type macrophages. (C) Quantification of CD163 expression level in the skin invasion front in different groups. Data are presented as the median and IQR, n=4. Statistical analysis was performed using the Kruskal-Wallis test followed by Dunn's test. \*P<0.05 and \*\*\*\*P<0.0001. ns, not significant (P>0.05); OSCC, oral squamous cell carcinoma; VSCC-SCs, verrucous squamous cell carcinoma-associated stromal cells; SCC-SCs, squamous cell carcinoma-associated stromal cells; HDFs, human dermal fibroblasts; TAMs, tumor-associated macrophages.

## Discussion

TAMs, as the main component of the TME, can regulate the angiogenesis, invasion and migration of cancers by secreting relevant factors. In addition, TAMs are involved in cancer

immunotherapy, such as checkpoint inhibitor therapy, adoptive cell transfusion, and cancer vaccine therapy. For the targeting of TAMs, there are three different strategies: The elimination of TAMs, the inhibition of monocyte recruitment and the reprogramming of TAMs. Therefore, TAMs particularly the



M2 type, are closely associated with the initiation and progression of cancer (28,29). In the majority of cancer models, TAMs are derived mainly from the differentiation of monocytes in peripheral blood (30,31). M2 type TAMs are closely associated with MVD in pancreatic ductal adenocarcinoma, and can be detected by CD31 and CD34 (32,33). Thus, it was hypothesized that the increased MVD may also influence the number of monocytes recruited by the crosstalk between cancer and stroma. In the present study, CD34 was used to examine the MVD in the skin invasion front, central area and bottom invasion front of OSCC, which suggested that the crosstalk between VSCC-SCs/SCC-SCs and HSC-3 cells promoted the MVD in skin invasion front, central area and bottom invasion front of OSCC, and that the crosstalk between SCC-SCs and HSC-3 cells exerted a more prominent promoting effect than the crosstalk between VSCC-SCs and HSC-3 cells. These data indicated that the crosstalk between cancer and the stroma promoted the infiltration of macrophages into the TME of OSCC by promoting MVD, and SCC-SCs exerted a more prominent promoting effect than VSCC-SCs. CD45 was used to label the monocytes to examine the effects of VSCC-SCs, SCC-SCs and HDFs on the infiltration of CD45(+) monocytes. The results revealed that the crosstalk between SCC-SCs and HSC-3 exerted a more prominent promoting effect on the infiltration of CD45(+) monocytes into the TME of OSCC than VSCC-SCs in the skin invasion front, whereas there was a minimal difference in the bottom invasion front, which may be caused by the complex structures in the bottom invasion front.

A recent study indicated that TAMs may be reliable markers to assay the aggressiveness of OSCC (34). In addition, CAFs can promote monocyte differentiation and the activation by secreting IL6 and GM-CSF (35). Thus, both cancer cells and CAFs may possibly promote the activation of TAMs in the TME. In the present study, the crosstalk between SCC-SCs and HSC-3 cells exerted a more prominent promoting effect on the activation and fusion of macrophages than VSCC-SCs *in vitro*. The size of macrophages increased following activation by the crosstalk between SCC-SCs and HSC-3 cells. After the fusion of macrophages, not only will the size of cells enlarge, but the number of nuclei will also increase. Furthermore, IF staining was used to evaluate F4/80 and CD163 expression to identify the characteristics of activated macrophages and multinucleated giant cells. These results suggested that the characteristics of these two cell types were similar to M2 type TAMs. In addition, MTS assay was used to assay the proliferative ability in the different groups, which demonstrated that both the VSCC-SCs and SCC-SCs inhibited the proliferation of macrophages, and the SCC-SCs exerted a more prominent promoting effect than the VSCC-SCs. Both the VSCC-SCs and SCC-SCs promoted macrophage proliferation following crosstalk with HSC-3 cells *in vitro* on days 2 and 3. Following crosstalk with HSC-3, the effect of SCC-SCs on the proliferation of macrophages significantly increased, whereas the effect of VSCC-SCs on the proliferation of macrophages decreased significantly. Based on Giemsa staining, IF and MTS assay, both the VSCC-SCs and SCC-SCs primarily promoted the activation and differentiation of macrophages into M2 type TAMs and SCC-SCs exerted a more prominent promoting effect than VSCC-SCs. Following crosstalk with HSC-3 cells, both VSCC-SCs and SCC-SCs mainly promoted the

proliferation and differentiation of macrophages into M2 type TAMs with SCC-SCs exerting a more prominent promoting effect than VSCC-SCs. In addition, the effects of VSCC-SCs and SCC-SCs on the migration of macrophages increased significantly following crosstalk with HSC-3 cells *in vitro*, and the SCC-SCs exerted a more prominent effect than the VSCC-SCs in promoting changes in the shape of macrophages from a spindle to a round shape. Based on Giemsa staining, the round-shaped macrophages were activated macrophages compared with spindle-shaped macrophages. It is considered that the spindle-shaped macrophages were more closely associated with the migration ability. After migration, the crosstalk between cancer and different subtype cancer stroma could induce the activation of macrophages, resulting in morphological changes from a spindle to a round shape. The number of round-shaped macrophages in the RAW264.7 + HSC-3 + SCC-SCs group was the highest, followed by that in the RAW264.7 + HSC-3 + VSCC-SCs group. Therefore, both the VSCC-SCs and SCC-SCs had a similar effect on the migration of macrophages, and the SCC-SCs had a more prominent effect on the activation of macrophages than the VSCC-SCs following crosstalk with HSC-3 cells *in vitro*.

Given that the pre-macrophages (BMDCs) and macrophages are CD11b(+) (36), IHC staining was used to observe CD11b expression to determine the effects of VSCC-SCs and SCC-SCs on the infiltration of CD11b(+) M0 type macrophages into the TME of OSCC following crosstalk with HSC-3 cells *in vivo*. The crosstalk between SCC-SCs and HSC-3 exerted a more prominent promoting effect on the infiltration of CD11b(+) TAMs than VSCC-SCs in the skin and bottom invasion fronts, while HDFs exerted a minimal effect. M2 type TAMs have anti-inflammatory and pro-tumor functions, and IHC staining can be used to examine the expression of CD206 and CD163 to assay the infiltration of M2 type TAMs into the TME of OSCC (37). Recent studies have indicated that OSCC-derived exosomes and CAFs play crucial roles in the polarization and infiltration of M2 type TAMs (38,39). Previous studies by the authors indicated that both VSCC-SCs and SCC-SCs promoted the progression of OSCC, which was more relevant with the M2 type TAMs rather than M1 type TAMs (19,20). Thus, the present study mainly focused on M2 type macrophages and did not perform staining for M1 markers to examine the M2/M1 ratio. In the present study, the crosstalk between SCC-SCs and HSC-3 cells exerted a more prominent promoting effect on the infiltration of CD163(+) M2 type TAMs in the skin invasion front than VSCC-SCs, whereas the HDFs exerted a minimal effect. However, there was a negative result in the bottom invasion front, which may be caused by complex structures such as bone, muscle and brain in bottom invasion front. In a previous study by the authors, it was reported that the cancer stroma promotes bone destruction by inducing osteoclasts on the bone surface (23). In addition, it was found that crosstalk between HSC-3 cells and VSCC-SCs/SCC-SCs promoted the fusion of macrophages into multinucleated giant cells. Therefore, it was hypothesized that factors released from the bone destroyed by the cancer/stroma complex caused the assembled macrophages to differentiate into osteoclasts or promote the fusion of macrophages into multinucleated giant cells rather than M2 macrophages. Given that the VSCC-SCs and SCC-SCs can promote the proliferation and migration of

macrophages following crosstalk with HSC-3 cells *in vitro*, the VSCC-SCs and SCC-SCs have immense potential to promote the infiltration of TAMs, by promoting the proliferation and migration following crosstalk with HSC-3 cells *in vivo*. In addition, after being mixed with HSC-3 cells to construct the animal model, the VSCC-SCs and SCC-SCs gradually disappeared. Therefore, it is quite difficult to determine whether the VSCC-SCs and SCC-SCs changed into cancerous cells through mesenchymal transition or provide the room for the direct infiltration of TAMs through the blood vessels inside the tumor.

IL1B plays a crucial role in the crosstalk between TAMs and multitype cancers; however, it has been poorly investigated in OSCC (40-42). It has been shown that the expression of BMP4 in TAMs is increased following co-culture with cancer cells, which in turn enhanced the invasion of gastric cancer cells (43). The TGF- $\beta$ /BMP signaling pathway also plays a key role in the crosstalk between pancreatic cancer and TAMs (44). Therefore, BMP4 may be involved in the differential effects of VSCC-SCs and SCC-SCs on the infiltration of TAMs into the TME of OSCC. IL6 was closely associated with the polarization of M2 type TAMs and OSCC progression, which may be involved in the differential effects of VSCC-SCs and SCC-SCs on the infiltration of TAMs into the TME of OSCC (45). CAFs can recruit M2 type TAMs by secreting CXCL12 in the TME of OSCC, which may be involved in the differential effects of VSCC-SCs and SCC-SCs on the infiltration of TAMs into the TME of OSCC (39).

In conclusion, the present study demonstrated that both VSCC-SCs and SCC-SCs promoted the differentiation, proliferation and migration of macrophages following crosstalk with HSC-3 cells *in vitro*. In addition, both VSCC-SCs and SCC-SCs promoted the MVD and infiltration of CD45(+) monocytes, CD11b(+) M0 type macrophages, and CD163(+) M2 type TAMs into the TME of OSCC following crosstalk with HSC-3 cells *in vivo*. The SCC-SCs exerted a more prominent promoting effect than the VSCC-SCs. Finally, IL1B, BMP4, IL6, and CXCL12 may be involved in the differential effects of VSCC-SCs and SCC-SCs on the infiltration of TAMs. These findings provide a potential regulatory mechanism underlying the effects of the cancer stroma on the infiltration of TAMs into the TME of OSCC, which may contribute to the development of novel treatment strategies for patients with OSCC by targeting TAMs.

### Acknowledgements

Not applicable.

### Funding

The present study was supported by the Japan Society for Promotion of Science (JSPS) KAKENHI Grants-in-Aid for Scientific Research (nos. JP20K10094, JP21K10043, JP21K17089, JP19K19159, JP20H03888 and JP22K10170).

### Availability of data and materials

The datasets generated and/or analyzed during the current study are available in the Gene Expression Omnibus

repository (<https://www.ncbi.nlm.nih.gov/geo/query/acc.cgi?acc=GSE164374>).

### Author's contributions

QS designed the outline of the study. All authors (QS, KT, HK, MWO, SS, MF, KN and HN) conducted experiments and data analysis. QS and KT were involved in the preparation of the manuscript. QS wrote the manuscript. KN, KN and HN supervised the study and contributed to data interpretation and manuscript revision. KT, KN and HN confirmed the authenticity of all raw data. All authors have read and agreed to the published version of the manuscript.

### Ethics approval and consent to participate

The present study was approved by the Ethics Committee of Okayama University (project identification code: 1703-042-001). Written informed consent was obtained from all patients. All animal experiments were conducted according to the relevant guidelines and regulations approved by the institutional committees at Okayama University (approval no. OKU-2017406).

### Patient consent for publication

Not applicable.

### Competing interests

The authors declare that they have no competing interests.

### References

1. Bray F, Ferlay J, Soerjomataram I, Siegel RL, Torre LA and Jemal A: Global cancer statistics 2018: GLOBOCAN estimates of incidence and mortality worldwide for 36 cancers in 185 countries. *CA Cancer J Clin* 68: 394-424, 2018.
2. Siegel RL, Miller KD and Jemal A: Cancer statistics, 2016. *CA Cancer J Clin* 66: 7-30, 2016.
3. Coussens LM and Werb Z: Inflammation and cancer. *Nature* 420: 860-867, 2002.
4. Watanabe T, Kamio N, Okabe T, Hayama T, Fukai J, Watanabe A, Okada H and Matsushima K: Macrophage migration inhibitory factor promotes inflammation in human dental pulp. *J Hard Tissue Biol* 29: 9-16, 2020.
5. Suzuki T, Hayakawa T and Gomi K: GM-CSF stimulates mouse macrophages and causes inflammatory effects *in vitro*. *J Hard Tissue Biol* 28: 37-42, 2019.
6. Noy R and Pollard JW: Tumor-associated macrophages: From mechanisms to therapy. *Immunity* 41: 49-61, 2014.
7. Ruffell B, Affara NI and Coussens LM: Differential macrophage programming in the tumor microenvironment. *Trends Immunol* 33: 119-126, 2012.
8. Yamagata Y, Tomioka H, Sakamoto K, Sato K, Harada H, Ikeda T and Kayamori K: CD163-positive macrophages within the tumor stroma are associated with lymphangiogenesis and lymph node metastasis in oral squamous cell carcinoma. *J Oral Maxillofac Surg* 75: 2144-2153, 2017.
9. He KF, Zhang L, Huang CF, Ma SR, Wang YF, Wang WM, Zhao ZL, Liu B, Zhao YF, Zhang WF and Sun ZJ: CD163+ tumor-associated macrophages correlated with poor prognosis and cancer stem cells in oral squamous cell carcinoma. *Biomed Res Int* 2014: 838632, 2014.
10. Qian BZ and Pollard JW: Macrophage diversity enhances tumor progression and metastasis. *Cell* 141: 39-51, 2010.
11. Mills CD: M1 and M2 macrophages: Oracles of health and disease. *Crit Rev Immunol* 32: 463-488, 2012.

12. Goswami KK, Ghosh T, Ghosh S, Sarkar M, Bose A and Baral R: Tumor promoting role of anti-tumor macrophages in tumor microenvironment. *Cell Immunol* 316: 1-10, 2017.
13. Kai K, Moriyama M, Haque ASMR, Hattori T, Chinju A, Hu C, Kubota K, Miyahara Y, Kakizoe-Ishiguro N, Kawano S and Nakamura S: Oral squamous cell carcinoma contributes to differentiation of monocyte-derived tumor-associated macrophages via PAI-1 and IL-8 production. *Int J Mol Sci* 22: 9475, 2021.
14. Alves A, Diel L, Ramos G, Pinto A, Bernardi L, Yates J III and Lamers M: Tumor microenvironment and oral squamous cell carcinoma: A crosstalk between the inflammatory state and tumor cell migration. *Oral Oncol* 112: 105038, 2021.
15. Schmid MC, Khan SQ, Kaneda MM, Pathria P, Shepard R, Louis TL, Anand S, Woo G, Leem C, Faridi MH, *et al*: Integrin CD11b activation drives anti-tumor innate immunity. *Nat Commun* 9: 5379, 2018.
16. Patel SG and Shah JP: TNM staging of cancers of the head and neck: Striving for uniformity among diversity. *CA Cancer J Clin* 55: 242-264, 2005.
17. Spiro RH, Guillaumondegui O Jr, Paulino AF and Huvos AG: Pattern of invasion and margin assessment in patients with oral tongue cancer. *Head Neck* 21: 408-413, 1999.
18. Hussein MR and Cullen K: Molecular biomarkers in HNSCC: Prognostic and therapeutic implications. *Expert Rev Anticancer Ther* 1: 116-124, 2001.
19. Takabatake K, Kawai H, Omori H, Qiusheng S, Oo MW, Sukegawa S, Nakano K, Tsujigiwa H and Nagatsuka H: Impact of the stroma on the biological characteristics of the parenchyma in oral squamous cell carcinoma. *Int J Mol Sci* 21: 7714, 2020.
20. Shan Q, Takabatake K, Omori H, Kawai H, Oo MW, Nakano K, Ibaragi S, Sasaki A and Nagatsuka H: Stromal cells in the tumor microenvironment promote the progression of oral squamous cell carcinoma. *Int J Oncol* 59: 72, 2021.
21. Sakakura K, Takahashi H, Kaira K, Toyoda M, Murata T, Ohnishi H, Oyama T and Chikamatsu K: Relationship between tumor-associated macrophage subsets and CD47 expression in squamous cell carcinoma of the head and neck in the tumor microenvironment. *Lab Invest* 96: 994-1003, 2016.
22. Dan H, Liu S, Liu J, Liu D, Yin F, Wei Z, Wang J, Zhou Y, Jiang L, Ji N, *et al*: RACK1 promotes cancer progression by increasing the M2/M1 macrophage ratio via the NF- $\kappa$ B pathway in oral squamous cell carcinoma. *Mol Oncol* 14: 795-807, 2020.
23. Shan Q, Takabatake K, Kawai H, Oo MW, Inada Y, Sukegawa S, Fushimi S, Nakano K and Nagatsuka H: Significance of cancer stroma for bone destruction in oral squamous cell carcinoma using different cancer stroma subtypes. *Oncol Rep* 47: 81, 2022.
24. Flecknell PA: *Laboratory Animal Anesthesia*. 3rd edition. Academic Press, San Diego, CA, 2009.
25. Adams S and Pacharinsak C: Mouse anesthesia and analgesia. *Curr Protoc Mouse Biol* 5: 51-63, 2015.
26. An YZ, Cho E, Ling J and Zhang X: The Axin2-snail axis promotes bone invasion by activating cancer-associated fibroblasts in oral squamous cell carcinoma. *BMC Cancer* 20: 987, 2020.
27. Wei C, Yang C, Wang S, Shi D, Zhang C, Lin X, Liu Q, Dou R and Xiong B: Crosstalk between cancer cells and tumor associated macrophages is required for mesenchymal circulating tumor cell-mediated colorectal cancer metastasis. *Mol Cancer* 18: 64, 2019.
28. Duan Z and Luo Y: Targeting macrophages in cancer immunotherapy. *Signal Transduct Target Ther* 6: 127, 2021.
29. Xiang X, Wang J, Lu D and Xu X: Targeting tumor-associated macrophages to synergize tumor immunotherapy. *Signal Transduct Target Ther* 6: 75, 2021.
30. Cassetta L, Fragkogianni S, Sims AH, Swierczak A, Forrester LM, Zhang H, Soong DYH, Cotechini T, Anur P, Lin EY, *et al*: Human tumor-associated macrophage and monocyte transcriptional landscapes reveal cancer-specific reprogramming, biomarkers, and therapeutic targets. *Cancer Cell* 35: 588-602.e10, 2019.
31. Devalaraja S, To TKJ, Folkert IW, Natesan R, Alam MZ, Li M, Tada Y, Budagyan K, Dang MT, Zhai L, *et al*: Tumor-derived retinoic acid regulates intratumoral monocyte differentiation to promote immune suppression. *Cell* 180: 1098-1114.e16, 2020.
32. Yang Y, Guo Z, Chen W, Wang X, Cao M, Han X, Zhang K, Teng B, Cao J, Wu W, *et al*: M2 macrophage-derived exosomes promote angiogenesis and growth of pancreatic ductal adenocarcinoma by targeting E2F2. *Mol Ther* 29: 1226-1238, 2021.
33. Miyata Y, Kanda S, Ohba K, Nomata K, Hayashida Y, Eguchi J, Hayashi T and Kanetake H: Lymphangiogenesis and angiogenesis in bladder cancer: Prognostic implications and regulation by vascular endothelial growth factors-A, -C, and -D. *Clin Cancer Res* 12(3 Pt 1): 800-806, 2006.
34. Mukherjee A, Spadigam A and Dhupar A: Tumor-associated macrophages: Harbingers of aggressiveness in oral squamous cell carcinoma. *J Oral Maxillofac Pathol* 25: 46-50, 2021.
35. Cho H, Seo Y, Loke KM, Kim SW, Oh SM, Kim JH, Soh J, Kim HS, Lee H, Kim J, *et al*: Cancer-stimulated CAFs enhance monocyte differentiation and protumoral TAM activation via IL6 and GM-CSF secretion. *Clin Cancer Res* 24: 5407-5421, 2018.
36. Okubo M, Kioi M, Nakashima H, Sugiura K, Mitsudo K, Aoki I, Taniguchi H and Tohnai I: M2-polarized macrophages contribute to neovasculogenesis, leading to relapse of oral cancer following radiation. *Sci Rep* 6: 27548, 2016.
37. Weber M, Moebius P, Büttner-Herold M, Amann K, Preidl R, Neukam FW and Wehrhan F: Macrophage polarisation changes within the time between diagnostic biopsy and tumour resection in oral squamous cell carcinomas-an immunohistochemical study. *Br J Cancer* 113: 510-519, 2015.
38. Pang X, Wang SS, Zhang M, Jiang J, Fan HY, Wu JS, Wang HF, Liang XH and Tang YL: OSCC cell-secreted exosomal CMTM6 induced M2-like macrophages polarization via ERK1/2 signaling pathway. *Cancer Immunol Immunother* 70: 1015-1029, 2021.
39. Li X, Bu W, Meng L, Liu X, Wang S, Jiang L, Ren M, Fan Y and Sun H: CXCL12/CXCR4 pathway orchestrates CSC-like properties by CAF recruited tumor associated macrophage in OSCC. *Exp Cell Res* 378: 131-138, 2019.
40. Eum HH, Kwon M, Ryu D, Jo A, Chung W, Kim N, Hong Y, Son DS, Kim ST, Lee J, *et al*: Tumor-promoting macrophages prevail in malignant ascites of advanced gastric cancer. *Exp Mol Med* 52: 1976-1988, 2020.
41. Chittezhath M, Dhillon MK, Lim JY, Laoui D, Shalova IN, Teo YL, Chen J, Kamaraj R, Raman L, Lum J, *et al*: Molecular profiling reveals a tumor-promoting phenotype of monocytes and macrophages in human cancer progression. *Immunity* 41: 815-829, 2014.
42. Chen Q, Wang J, Zhang Q, Zhang J, Lou Y, Yang J, Chen Y, Wei T, Zhang J, Fu Q, *et al*: Tumour cell-derived debris and IgG synergistically promote metastasis of pancreatic cancer by inducing inflammation via tumour-associated macrophages. *Br J Cancer* 121: 786-795, 2019.
43. Shen Z, Kauttu T, Cao J, Seppänen H, Vainionpää S, Ye Y, Wang S, Mustonen H and Puolakkainen P: Macrophage coculture enhanced invasion of gastric cancer cells via TGF- $\beta$  and BMP pathways. *Scand J Gastroenterol* 48: 466-472, 2013.
44. Shen Z, Seppänen H, Kauttu T, Vainionpää S, Ye Y, Wang S, Mustonen H and Puolakkainen P: Vasohibin-1 expression is regulated by transforming growth factor- $\beta$ /bone morphogenic protein signaling pathway between tumor-associated macrophages and pancreatic cancer cells. *J Interferon Cytokine Res* 33: 428-433, 2013.
45. Petrucci MN, Cherubini K, Salum FG and de Figueiredo MA: Role of tumour-associated macrophages in oral squamous cells carcinoma progression: An update on current knowledge. *Diagn Pathol* 12: 32, 2017.



This work is licensed under a Creative Commons Attribution-NonCommercial-NoDerivatives 4.0 International (CC BY-NC-ND 4.0) License.